Transparent Flexible Plastic Substrates for Organic Light-Emitting Devices

YONGTAEK HONG,[1] ZHIQI HE,[1,4] NANCY S. LENNHOFF,[2] DAVID A. BANACH,[3] and JERZY KANICKI[1,5,6]

1.—Solid-State Electronics Laboratory, Department of EECS, University of Michigan, Ann Arbor, MI 48109 2.—3M Touch Systems, Methuen, MA 01844. 3.—Department of Chemistry and Materials, University of California, Santa Barbara, CA 93105. 4.—Currently at Optrex America, Plymouth, MI 48170. 5.—Also with the Center for Polymers and Organic Solids, University of California, Santa Barbara, CA 93105. 6.—E-mail: kanicki@eecs.umich.edu

In this paper, we describe the properties of flexible plastic substrates with a transparent conducting electrode (TCE), which are important for organic light-emitting devices (OLEDs). Specifically, we have evaluated the TCE electrical resistivity, surface roughness, electrode patterning, optical transmission, and the substrate water vapor/oxygen transmission. We have studied the effect of ultraviolet (UV)-ozone treatment on the TCE surface by using contact angle measurements and x-ray photoelectron spectroscopy (XPS). A decrease in the advancing contact angle by 30–40° and an increase of oxygen content on the TCE surface by 10 at.% were observed after the UV-ozone treatment. These changes facilitate the polymer adhesion to the TCE surface and increase the TCE surface work function, respectively. A sheet resistance of 12–13 $\Omega/\square$, an optical transmission greater than 80% over the visible range, and a surface roughness of 1.4–2.2-nm RMS over 50×50 μm^2 have been obtained for the plastic substrates. These properties are adequate for OLED applications based on United States Display Consortium specifications. Finally, we have found that a combination of hydrogenated amorphous silicon-nitride and silicon-oxide layers deposited on one side of the substrate at low-temperature reduces the water vapor and oxygen transmission rates (TRs) to less than 10^{-5} g/cm²-day-atm and about 10^{-7} cc/cm²-day-atm, respectively.

Key words: Plastic substrate, organic light-emitting device, gas transmission rate, transparent conducting electrode

INTRODUCTION

Organic light-emitting devices (OLEDs) are now being considered as the next-generation flat panel displays (FPDs) for such applications as smart identification cards, screens of mobile units, and vehicular displays. This is because OLEDs have several advantages, such as low operating voltage, low power consumption, self-emission, fast response time, large viewing angle, high luminous efficiency, ultrathin structure, and light weight.[1,2] However, so far, most OLEDs have been built on rigid glass or silicon substrates, even though the low-cost, low-temperature

processing of the OLEDs renders them as one of the most promising candidates for the display implementation on flexible plastic substrates. Plastic substrates have several distinct advantages, such as ruggedness, robustness, ultra lightness, conformability, and impact resistance over glass substrates, which are primarily used in FPDs today.[3,4] Furthermore, their flexibility becomes a very attractive feature as the OLED technology matures.[5–8] However, high transparency, proper surface roughness, low gas permeability, and high transparent electrode conductivity of the plastic substrate are required for commercial applications.

Mahon et al.[9] have reported several important properties of plastic substrates coated with a trans-

parent conducting electrode (TCE), which are required for OLED display applications. Based on this paper and research supported by the United States Display Consortium, plastic substrates should have a transparency greater than 95% with less than 0.5% haze over the visible range, a surface roughness less than 2-nm RMS, a gas permeability of less than 10^{-6} g/m²-day and 10^{-7} cc/m²-day-atm for water vapor and oxygen, respectively, and a sheet resistance of less than 50 $\Omega/\square$, preferably about 10 $\Omega/\square$. The plastic substrate should also be stable under heat, humidity, and ultraviolet (UV) light. The substrate hardness should be >6H, and the cost should be <60 USD/m². Especially, for OLEDs whose operating stability is very sensitive to water vapor and oxygen, a low permeability of water vapor and oxygen through the substrate is a critical requirement,[10,11] which is very difficult to achieve.

Initial studies of flexible plastic substrates for OLEDs were focused on polyester[12,13] and poly (ethylene terephthalate)[14,15] because of their low cost and proper optical properties. However, the use of such plastic substrates is not possible in active-matrix displays because the pixel electrode circuits need to be fabricated at temperatures higher than the glass-transition temperature of these substrates. In addition, the thermal expansion coefficient of the substrates is much higher than that of silicon. Therefore, the high-temperature process leads to considerable mechanical stress and difficulties in maintaining accurate alignment of features on the plastic substrate. These problems are particularly severe for polysilicon, active-matrix pixel electrode circuits.

To address these issues, we have chosen as the base film for our substrates the poly (bis (cyclopentadiene) condensate, such as the material sold by LOFO High Tech Film (Weilam Rhein, Germany) under the trade name TRANSPHAN OG.[16] LOFO (old Lonza) cast TRANSPHAN OG from a solution of Arton G in methylene chloride. The resin Arton G was purchased from Japan Synthetic Rubber Co. Ltd. (Tokyo); its chemical formula is shown in Fig. 1a.

The objective of this paper is to report on the properties of the flexible plastic substrates used in this study. These properties, relevant to OLEDs, are compared with the requirements of the plastic substrates for OLED applications, which are summarized in Table III. For any practical display applications, these requirements must be satisfied.

EXPERIMENTAL DETAILS AND RESULTS

Structure of the Multilayer Flexible Plastic Substrate

Fig. 1a and b shows a schematic structure and a transmission electron microscope (TEM) cross section of "dry-etchable" plastic substrates. The "wet-etchable" substrate has only one barrier layer between bottom indium tin oxide (ITO) and hard coat layers,
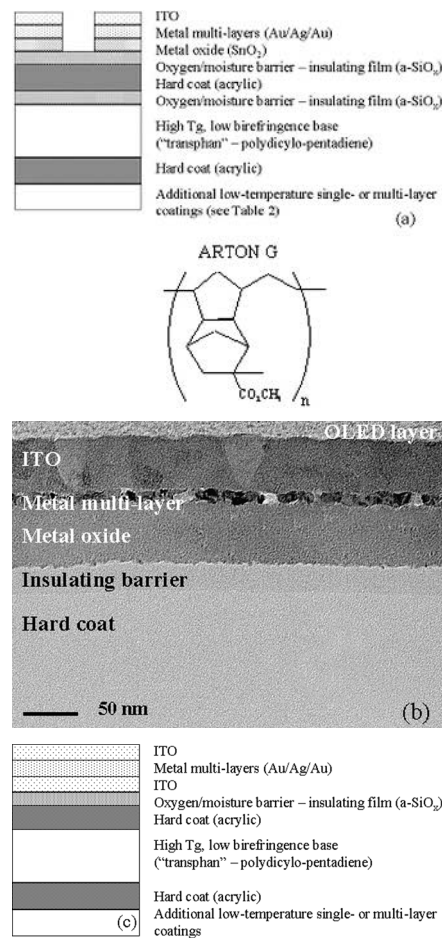
Fig. 1. (a) and (c) Schematic structure of the multilayer dry- and wet-etchable flexible plastic substrates[17–19] and (b) TEM image of the dry-etchable plastic substrate cross section.

as shown in Fig. 1c. A multilayer composition for both substrates is very similar. We define dry-etchable and wet-etchable plastic substrates as the plastic substrate coated with a TCE that can be etched either by a laser-based method (dry-etchable)[17,18] or by a wet chemical process (wet-etchable),[19] respectively.

The TCE consists of a semitransparent, thin multilayer metal (for example, Au/Ag/Au) sandwiched between the top ITO and bottom metal. For dry-etchable and wet-etchable substrates, tin oxide (SnO₂) and ITO were used for the bottom metal oxide, respectively. This multilayer structure improves the TCE conductivity without significantly affecting the optical transmission through the plastic substrate. It is well known that a very thin silver or silver-containing palladium layer between the transparent-conducting oxide layers allows for very high electrical conductivity, good mechanical durability, and high transparency in the visible range because of the anti-reflection effect.[20] We have also observed a similar effect for our TCE structure, which is described in a later section.

To enhance the substrate thermal and mechanical stability, optical characteristics, and gas-blocking property, a multilayer structure was used on both

sides of a high glass-transition temperature (T_g), low-birefringence base film. The acrylic and low-temperature amorphous silicon oxide (a-SiOx) was used as a hard coat and oxygen/moisture barrier, respectively.[17–19] To further reduce the water vapor and oxygen transmission through the plastic substrate, additional layers have been deposited on one side of the plastic substrate, which are indicated as additional low-temperature coating layers in Fig. 1a. Their impact on substrate properties will be discussed in a later section.

The TCE Surface (Top ITO) Composition

Table I shows the chemical compositions of the top ITO surface for the wet-etchable[19] plastic substrates before and after the UV-ozone treatment ($\sim$20 min), which were determined by x-ray photoelectron spectroscopy (XPS). The Al K_α radiation (hv = 1,486.6 eV) under a high vacuum (10^{-9} torr) was used to obtain O_{1s}, C_{1s}, In_{3d}, and Sn_{3d} core-level spectra. A charge neutralizer was used for all samples. Survey and high-resolution scans were measured at pass energies of 160 eV and 10 eV, respectively. The take-off angle for all samples was 90°. The O_{1s} peaks for all ITO samples have been deconvoluted into three peaks, In_2O_3, $In(OH)_3$, and $InOOH$, and surface contaminants from the photoemission process, i.e., H_2O, CO_2, etc. The last contribution to the O_{1s} peak dements the correct oxygen concentration actually bound to the metal and, therefore, must be removed before calculating elemental concentrations. An Ar^+ sputtering was used to remove these contaminants, but Ar^+ may also remove some oxygen bound to the metal in the process. To obtain an accurate profile of the oxygen actually bound to the metal, two high-resolution scans were taken of each sample. The first high-resolution scan was used for peak position determination. Then Ar^+ sputtering was applied until the C_{1s} peak disappeared because carbon is a source of atmospheric contamination in XPS. A second scan was used to confirm that the peak assigned to contaminants vanished after Ar^+ sputtering. Therefore, the contaminant component was subtracted out of the O_{1s} spectrum, and the elemental atomic concentrations for the ITO were then calcu-

lated using specific XPS software. To determine the oxygen stoichiometric ratio, the oxygen amount was related to indium and tin, and the value of $[O]/(1.5[In] + 2[Sn])$ was calculated. The ratios of $[Sn]/[In]$, $[Sn]/[O]$, and $[I]/[O]$ are also included in Table I.

From the experimental results, we can conclude that the peak intensity corresponding to the SnO_2-like species decreased, indicating a donor reduction and a change of Fermi level in the ITO with an energy bandgap. At the same time, the peak intensity corresponding to O_{1s} increased after the UV-ozone treatment. The intensity of this peak becomes even higher after an additional oxygen plasma treatment was performed on the TCE surface. The oxygen can be bonded to In and Sn in the ITO, and its electron density is smaller than that of O^{2-} ions.[21] This increase can produce a reduced carrier concentration at the ITO surface, thereby decreasing the ITO surface conductivity.

We also observed carbon core signals in XPS for both substrates, which represent the common carbon contamination of the ITO surface as reported in the literature.[22] Therefore, surface treatment, such as oxygen plasma or UV ozone, needs to be performed before deposition of the organic layer, especially from an aqueous solution. This type of surface treatment will remove the contaminants, such as carbon, and render the ITO surface hydrophilic.[23,24] As indicated in Table I, the atomic concentration of C_{1s} decreased after the UV-ozone treatment. It is considered that carbon on the ITO surface was oxidized to C = O by UV-ozone treatment and, then, was pumped out by a vacuum pump.

At the same time, the UV-ozone or oxygen plasma treatment will increase the work function of ITO by 0.5–0.7 eV.[25] The ITO work function after such treatment is about 4.7–4.8 eV. The increase of the ITO work function can be due to the reduction of the carbon contamination at the ITO surface and the formation of a dipole layer resulting from a surface rich in negatively charged oxygen. The increase of the ITO work function enhances the carrier injection/extraction at the ITO/organic interface and improves the OLED performance.[25]

Table I. Top ITO Surface Chemical Composition of Wet-Etchable Plastic Substrates

Sample Description	O_2 Plasma Treatment (s)	Atomic Concentrations (%)				Stoichiometric Ratios			
		O_{1s}	C_{1s}	In_{3d}	$Sn_{3d5/2}$	Oxygen Stoichiometric Ratio*	[Sn]/[In]	[Sn]/[O]	[In]/[O]
ITO—wet-etchable before UV ozone	—	27.9	35.7	33.2	3.2	0.50	0.10	0.11	1.19
ITO—wet-etchable after UV ozone	—	30.26	29.11	35.9	3.46	0.50	0.10	0.09	1.19
ITO—wet-etchabl after UV ozone	30	37.51	21.63	35.37	3.48	0.63	0.10	0.09	0.94

* $[O]/(1.5[In] + 2[Sn])$—should be 1 theoretically.

Contact Angle of the TCE Surface (Top ITO)

Surface activation (oxygen plasma, corona, and UV-ozone treatment) is commonly used in the coating industry to increase the wettability of the substrate and the adhesion of the coating. The effect on the surface is almost the same for every pre-treatment method. The surface is oxidized, leading to the introduction of functional (such as hydroxyl, carboxylic, or carbonylic) groups and contributing to an increase of the surface energy. To obtain good wettability and adhesion, it is important that the surface energy of the substrate ($\gamma_{substrate}$) be at least equal to or higher than the surface energy of the liquid-coating material ($\gamma_{coating}$), i.e., $\gamma_{substrate} \geq \gamma_{coating}$. According to the Owens and Wendt (OW) approach,[26–28] the interaction forces arising from every liquid and solid material consist of two components, the disperse force and all polar interactions. The disperse component represents the nonpolar van der Waals (London) forces, while the polar interaction comprises the van der Waals forces involving, e.g., permanent dipoles as well as electrostatic interactions and hydrogen bond forces. The OW method states that the total surface energy of a solid (γ_s) is comprised of both polar (γ^p) and dispersive (γ^d) components and is equal to their sum: $\gamma_s = \gamma_s^p + \gamma_s^d$. The total surface energy is the driving force for the wetting of the ITO surface, and the polar component is important for the adhesion properties.

The standard method to measure the surface energy of a solid system is a contact angle measurement. The principle relates to the wettability of the solid surface by a group of specified liquids. As long as the surface energy of the liquid is significantly higher than that of the solid surface, the liquid will not spread over the surface but will form a drop with a specific angle to the solid phase. Based on the OW approach, it is possible to calculate the surface energy of solids from the contact angle and the surface tension of the test liquid used.

The surface tension is split into a disperse component and a polar component:

$$\gamma_{LV}(1+\cos\theta) = -2\left[\left(\gamma_S^d\gamma_{LV}^d\right)^{1/2} + \left(\gamma_S^p\gamma_{LV}^p\right)^{1/2}\right] \qquad (1)$$

where θ is the contact angle between the liquid and the surface, γ_{LV}^d and γ_{LV}^p are known values (given in Table II) for different liquids, and γ_{LV} is the sum of $\gamma_{LV}^d + \gamma_{LV}^p$. The two unknowns in Eq. 1 are γ_s^p and γ_s^d, which can be calculated by measuring the contact angle using two different liquids and solving Eq. 1 simultaneously for γ_s^p and γ_s^d.

Two standard liquids that can be used are deionized (DI) water (H_2O – DI) and diiodomethane or methylene iodine (CH_2I_2).[29] Because CH_2I_2 is a nonpolar liquid, the preceding equation can be simplified into

$$\gamma_{LV}(1+\cos\theta) = -2\left(\gamma_S^d\gamma_{VL}^d\right)^{1/2} \qquad (2)$$

Then, we can obtain both the disperse component (γ_s^d) and the polar component (γ_s^p) of the surface.

By summing these components, the total surface energy (γ_s) can be calculated.

Besides wettability and surface potential, surface polarity (P_s) is another important factor that influences the adhesion of the organic polymer to the ITO surface:

$$P_s = \frac{\gamma_S^p}{\gamma_S} \qquad (3)$$

The liquids used for the wetting experiments were distilled DI water and methylene iodine. Advancing contact angle measurements were performed by the sessel drop technique using a Ramé–Hart (Mountain Lakes, NJ) goniometer (Model A-100). The sessel drop was displaced onto the surface of the sample by a micrometric syringe and needle. The angle of the liquid drop on the surface is known as the contact angle. At least four contact angles were measured for each sample in different spots and averaged. The error associated with the contact angle measurement was ±~3°. All measurements were performed at room temperature in air.

The overall set of results from contact angle measurements on the ITO surface before and after UV-ozone treatment is given in Table II. As expected, after UV-ozone treatment, the ITO surface polarity and surface tension increased. The oxygen plasma treatment also showed a similar effect on the ITO surface, as shown in Table II. It should be noted that the polarity and surface tension of the organic polymers used in this research are lower than those of the ITO surface. This will ensure a good solvent wettability of the ITO surface, a good polymer adhesion to the ITO surface, and a good electrical contact between the ITO and the organic layer. Overall very reproducible optoelectronic properties of the OLEDs can be obtained using this system.

TCE Electrical and Optical Characteristics

Equally spaced (S = 0.159 cm) linear four-point probes[30] were used to measure sheet resistance of the TCE on the plastic substrate. To reduce any measurement error, 15 × 15 cm² electrode-coated substrates were used. In this method, a current range of 1–10 mA was applied between the two outer probes, and the voltage drop across the two inner probes was measured. The sheet resistance (R_S) was calculated using Eq. 4 with the slope extracted from the measured current-voltage characteristics, as shown in Fig. 2a because the electrode thickness (~1,000 Å < 0.1S) is small and the sample boundaries (15 cm > 40S) are large compared to the probe spacing (S).[31] When the thickness (d) of the conductive thin film is considered, the resistivity (ρ) can also be calculated:

$$R_S = 4.5324\frac{V}{I}\,(\Omega/\square) \qquad (4)$$

$$\rho = R_S \times d\,(\Omega\text{-cm}) \qquad (5)$$

Because of the unique structure of the TCE layer, a sheet resistance of about 12–13 $\Omega/\square$ has been

Table II. Contact Angle Measurement Results for Top ITO Surface of Dry-Etchable and Wet-Etchable Plastic Substrates

Reference Values	γ_{water} (dyn/cm) 72.8	γ_{water}^{d} (dyn/cm) 21.8	γ_{water}^{p} (dyn/cm) 51	$\gamma_{methyl\ iodide}$ (dyn/cm) 50.4	$\gamma_{methyl\ iodide}^{d}$ (dyn/cm) 50.02	$\gamma_{methyl\ iodide}^{p}$ (dyn/cm) 0.38
Samples	DI-H$_2$O θ (°)	CH$_2$I$_2$ θ (°)	γ_s (dyn/cm)	γ_s^d (dyn/cm)	γ_s^p (dyn/cm)	P$_s$
Dry-etchable ITO before UV ozone	102 ± 3.2	64.75 ± 2.8	25.7	25.2	0.57	0.022
Dry-etchable ITO after UV ozone	64.2 ± 4.6	48 ± 1.4	44.9	31.7	13.2	0.294
Wet-etchable ITO before UV ozone	99.6 ± 2.9	52.25 ± 1.9	32.8	32.5	0.27	0.008
Wet-etchable ITO after UV ozone	70.5 ± 3.5	41.75 ± 2.5	44.0	35.6	8.4	0.190
Wet-etchable ITO after oxygen plasma	56.2 ± 2.2	41.8 ± 2.6	51.2	34.4	16.8	0.330

obtained without any significant reduction of the optical transmission through the substrate.

Fig. 2b shows the plastic substrate, optical-transmission spectrum measured with a Cary (Walnut Creek, CA) UV-vis-NIR-Spectrophotometer, where air was used as a reference. An optical transmission greater than 80% over 450–750 nm ranges has been obtained, with maximum 85% and 86% for dry-etchable and wet-etchable plastic substrates, respectively. Better optical transmission of the plastic substrate compensates for slightly higher sheet resistance in comparison with the results (2 Ω/□ and average 70% optical transmission)[20] reported for a similar multilayer TCE deposited on glass substrates.

TCE Surface Roughness

Because a typical structure of OLEDs incorporates thin organic active layers (1,000–2,000 Å) deposited on an anode followed by cathode deposition, the surface roughness of the anode is critical for OLED optoelectronic performances.[9] If the surface is not smooth enough, the nonuniform electric-field distribution inside the device can trigger localized degradation.[22]

We used a contact-mode DI multimode, atomic force microscope (AFM) to investigate the surface roughness of the TCE on the plastic substrates,

where a 0.58 N/m^2 silicon-nitride cantilever was used at a 1-Hz scan rate. All the measured values were expressed as the root-mean-square values characterized by the following equation:

$$X_{RMS} = \sqrt{\frac{\Sigma(X_i - X_{ave})^2}{N}} \qquad (6)$$

where X$_i$, X$_{ave}$, and N are the measured values, average of the measured values, and total number of measurements for a specific area, respectively.

Fig. 3 shows the AFM images measured for 1×1 μm^2 TCE areas for both dry- and wet-etchable plastic substrates. From this figure, we obtained 1.1-nm RMS and 1-nm RMS values for the TCE on dry- and wet-etchable plastic substrates, respectively. We also measured the surface roughness over 50×50 μm^2 and obtained 2.2-nm RMS and 1.4-nm RMS values for dry- and wet-etchable plastic substrates, respectively. The measured RMS values are comparable to the surface roughness (less than 2 nm) required for the plastic substrate to be used for OLEDs (Table IV).[9]

TCE Patterning

Wet-chemical[32] and reactive ion etching[33] combined with photolithography and laser-based direct-write dry etching[34] methods have been used to
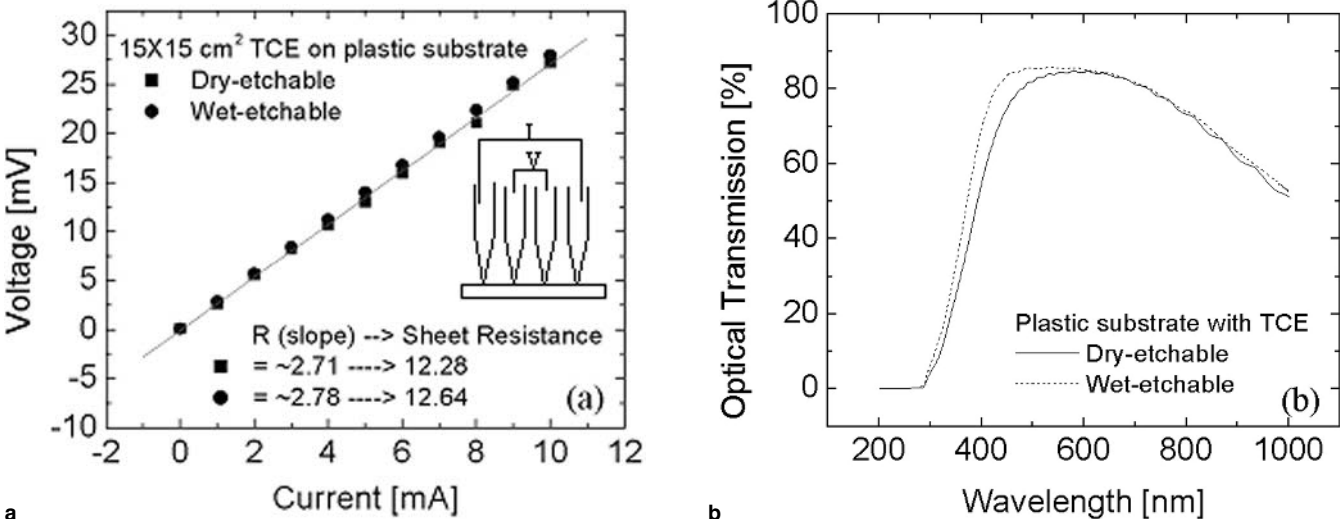
Fig. 2. (a) Electrical conductivity and (b) optical transmission of the dry-etchable and wet-etchable plastic substrates with TCE.
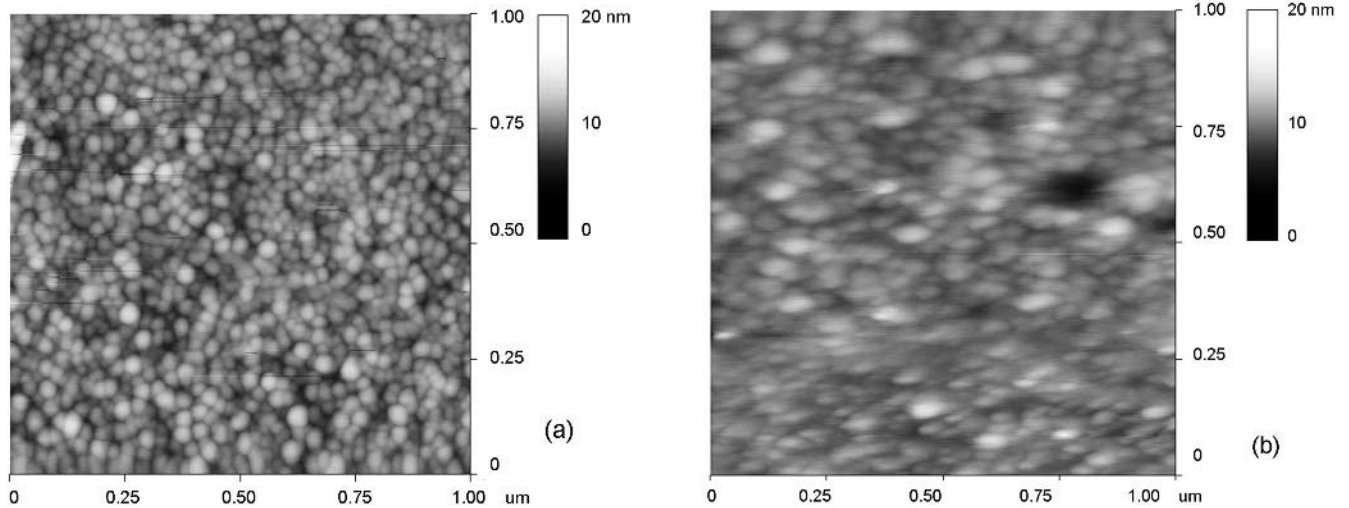
Fig. 3. AFM images of the TCE surface over 1×1 μm^2 area of (a) dry-etchable and (b) wet-etchable plastic substrates.

pattern ITO on glass substrates. Because no wet-chemical processes are needed for the laser-based, dry-etching method, this method was initially applied to pattern ITO on plastic substrates.[35] We also used the laser-based method to pattern the TCE on dry-etchable plastic substrates.[18] More recently, the wet-etching capability for TCE on wet-etchable plastic substrates was developed[19] and used in this study.

Because the TCE on the wet-etchable plastic substrate consists of the top ITO, metal multilayer, and bottom ITO, a specific etching solution[19] has been used, which is a 5:1 mixture of 3% H_2SO_4 and 0.01% $FeCl_3$. The wet etching was performed in an ultrasonic bath at 35°C. The evolution of the film thickness with etching time measured using a Dektak (Veeco Instruments, Woodbury, NY) 8000 profilometer is shown in Fig. 4. It is noted that there are three different etching rates, which can be associated with the top ITO, metal multilayer (Au/Ag/Au), and bottom ITO. The etching rates for the ITO extracted by using a least squares fitting method for 0–210 sec and 210–360 sec are found to be ~2.6 Å/sec and 2.5
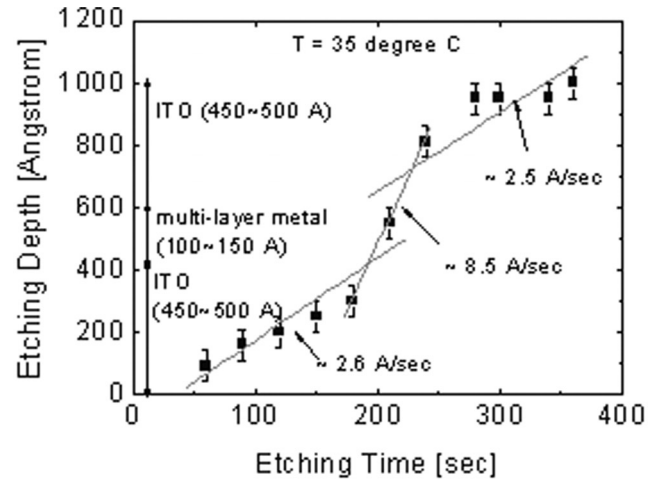
Fig. 4. Etching depth versus etching time characteristics of TCE on the wet-etchable plastic substrate.

Å/sec, respectively. The etching rate for the metal multilayer is extracted for 180–240 sec and is ~8.5 Å/sec. The change in etching rates is consistent with the TCE multilayer structure shown in Fig. 1c.

Table III. The TRs of the Water Vapor and Oxygen (TR$_{WV}$ and TR$_O$) through the Dry-Etchable Plastic Substrate Coated with Several Additional Low-Temperature Layers

Samples	TR$_{WV}$ (g/cm^2-day-atm)	TR$_O$ (cc/cm^2-day-atm)
Sample 1,500 Å a-SiN$_x$:H/1,500 Å a-SiO$_x$:H	$<1.55 \times 10^{-5}$*	2.53×10^{-7}
Sample 2,500 Å a-SiO$_x$:H	$<1.55 \times 10^{-5}$*	1.30×10^{-6}
Sample 2,500 Å a-SiN$_x$:H	3.74×10^{-5}	3.86×10^{-6}
Sample 400 Å Cr/2,000 Å Al	$<1.55 \times 10^{-5}$*	3.94×10^{-6}
Sample PPG	5.06×10^{-4}	2.13×10^{-5}
Blank TCE	1.17×10^{-4}	2.27×10^{-5}
Patterned TCE	3.66×10^{-4}	1.56×10^{-5}
Dry-etched**	$(1.2–9.4) \times 10^{-5}$	$(1.09–1.15) \times 10^{-5}$
Dry-unetched**	$(1.2–2) \times 10^{-5}$	$<5 \times 10^{-7}$
Wet-etched**	$(7.42–7.51) \times 10^{-5}$	$(3.87–3.89) \times 10^{-5}$
Wet-unetched**	$(0.49–1.02) \times 10^{-5}$	$(0.71–0.8) \times 10^{-5}$

* Measurement setup detection limit.
** Different measurement conditions are used: TR$_O$: 90% RH, 100% O_2, 0% RH, 100% N_2, 1 atm, 23°C; TR$_{WV}$: 100% RH, 0% RH, 1 atm, 23°C.

Table IV. Properties of the Flexible Plastic Substrate and Requirements for OLED Applications

Item	Description	Requirements[9]
R_S	12–13 Ω/□	<50 Ω/□ preferably <10 Ω/□
Optical transmission	>80% with <1% haze over visible range	>85% with <0.5% haze over visible range
Surface roughness	1–1.1-nm RMS over 1×1 μm^2 1.4–2.2-nm RMS over 50×50 μm^2	<2 nm RMS
Surface polarity	>0.25	N/A
Work function of transparent anode	~4.8 eV	N/A
Patterning capability	Dry-etchable: laser-based method Wet-etchable: chemical process → 3% H_2SO_4:0.01% $FeCl_3$ (5:1)	HCl:HNO_3:HF:H_2O (5:1:1:3) ITO etching, no attack on substrate
Chemical resistance	γ-Butyrolacetone, NMP, MEK, IPA, 10% NaOH, acetone, IPA, PR, PR stripper, detergent	acetone, methanol, IPA, NMP, TEC, standard PR, PR stripper, H_2O_2, NaOH, NH_4F
Heat resistance	Up to 145°C with 170°C glass-transition temperature	No change of physical and optical properties at 200°C for 1 h
TR_O*	1.56×10^{-5} cc/cm^2-day-atm $\leq 1.5 \pm 1 \times 10^{-7}$ cc/cm^2-day-atm (with a-SiN$_x$:H and a-SiO$_x$:H coating)	<10^{-7} cc/cm^2-day-atm
TR_{WV}*	3.66×10^{-4} g/cm^2-day-atm <10^{-5} g/cm^2-day-atm (below detection limit) (with a-SiN$_x$:H and a-SiO$_x$:H coating)	<10^{-6} g/cm^2-day-atm
Environmental stability	1,000 h at 90°C	100 h at 50°C, 90% RH 250 h at 100°C and −25°C
Thickness	100–188 μm	100–1,100 μm

* Only for dry-etchable plastic substrates.

Water Vapor and Oxygen-Transmission Analysis

Because organic materials used in OLED applications are sensitive to water vapor and oxygen, it is critical to protect the active organic layers from being exposed to water vapor and oxygen for better device operating stability and longer display lifetime.[10] Therefore, the plastic substrate must also have a very good gas-blocking property for OLED applications (Table IV).

The water vapor and oxygen transmission rates (TRs) (TR_{WV} and TR_O) through our dry-etchable plastic substrate were analyzed using the American Society for Testing and Material (ASTM) methodology.[36,37]

ASTM Measurement Details

Fig. 5 shows the experimental setup used to measure water vapor and oxygen TRs (TR_{WV} and TR_O) through the plastic substrate. The term TR_{WV} is the time rate of water vapor flow normal to the substrate surface per unit area under steady-state conditions, which was measured using a pulsed infrared sensor at a substrate temperature of 37.8°C. The "A side" of the chamber had 49-mmHg partial pressure, 100% relative humidity (RH) water vapor. The A side of the chamber was maintained at 100% RH during analysis. The "B side" of the chamber was about 0% RH before, during, and after analysis. When water vapor diffusing through the substrate
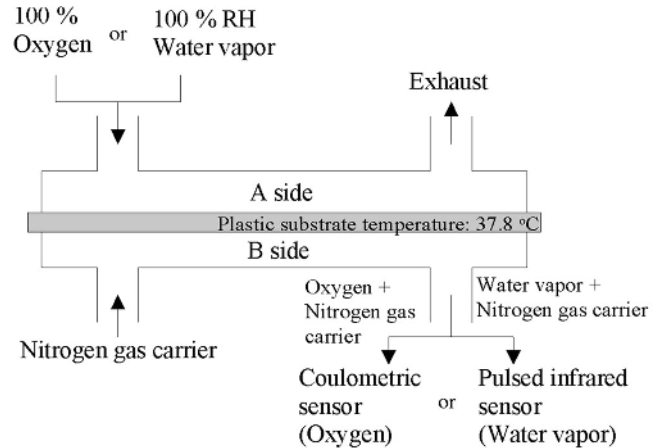
Fig. 5. Experimental setup used for TR_{WV} and TR_O of the plastic substrate. The pulsed infrared and Coulometric sensors are used to detect the amount of water vapor and oxygen diffusing from A side to B side through the substrate, respectively.

to the B side is carried into the infrared sensor, the sensor measures the fraction of infrared energy absorbed by the water vapor and produces an electrical signal, whose amplitude is proportional to the water-vapor concentration. The amplitude of the electrical signal measured for the plastic substrate is then compared to the signal produced from the calibration film of known TR.[37] The term TR_O is the quantity of oxygen gas passing through a unit area of the substrate under the test conditions, which was measured using a Coulometric sensor at a sub-
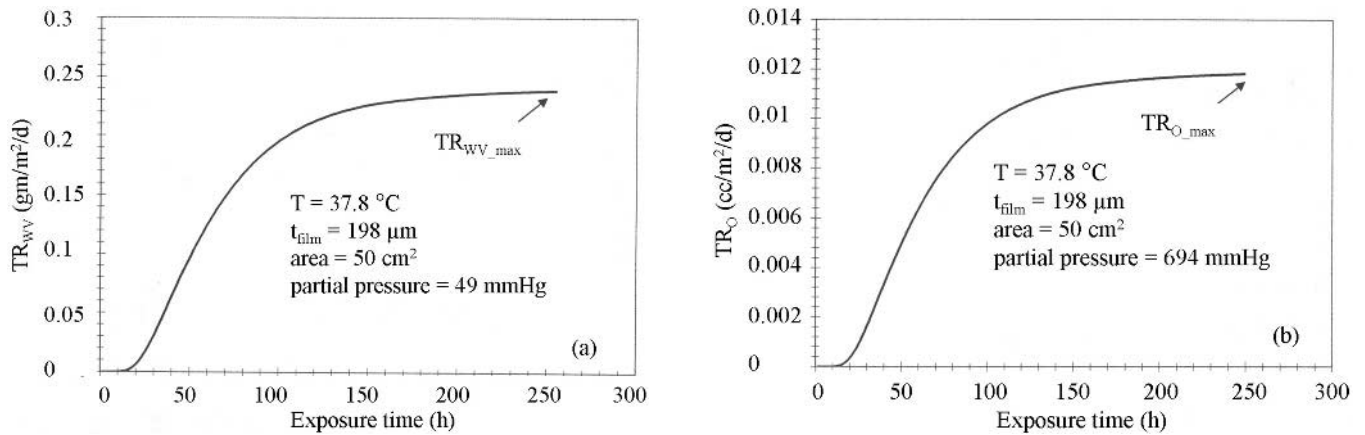
Fig. 6. Examples of (a) TR_{WV} and (b) TR_O characteristics versus gas-exposure time for the dry-etchable plastic substrate. Experimental conditions are also included in graphs. The TR saturates as gas-exposure time increases, and these saturated values represent the maximum TRs (TR_{max}), which are used to calculate TR_{WV} and TR_O of the plastic substrates.

strate temperature of 37.8°C.[36] The partial pressure of oxygen in the A side was measured during the analysis. The A side of the chamber had 100% oxygen at 90% RH during analysis. The B side of the chamber was maintained at 0% RH before, during, and after analysis. Because the Coulometric sensor is insensitive to water vapor, it measures only the amount of oxygen flowing into the detector and produces the corresponding electrical current. As shown in Fig. 5, the nitrogen carrier transports a water vapor or oxygen molecule diffusing through the substrate into the infrared or Coulometric sensor, respectively.

From the described experimental setup, the TR values for the plastic substrate can be obtained using the following procedure. First, the change of TR versus gas-exposure time is measured. Fig. 6 shows an example of the measured TR_{WV} and TR_O characteristics versus gas-exposure time for the plastic substrate. The TR saturates as gas-exposure time increases, and these saturated values represent the maximum TRs (TR_{max}). Using TR_{max}, TR values can be calculated as follows:

$$TR = TR_{max} \times P_{gas} \qquad (7)$$

where P_{gas} is the partial pressure in atm unit of water vapor or oxygen. From the preceding graphs, TR_{max} values are 0.241 g/m²-day and 0.0119 cc/m²-day for water vapor and oxygen, and the partial pressure values for water vapor and oxygen measurements are 49 mmHg and 694 mmHg; thus, TR_{WV} and TR_O of 3.74×10^{-4} g/cm²-day-atm and 1.3×10^{-6} cc/cm²-day-atm are obtained, respectively. By using this methodology, we analyzed the gas TRs for the plastic substrates coated with additional low-temperature layers, which will be discussed in the next subsection.

Measurement Results

Although the substrate has a multilayer structure to enhance the gas-blocking properties as shown in Fig. 1, 10^{-4}–10^{-6} g/cm²-day-atm and 10^{-5}–10^{-7}

cc/cm²-day-atm for TR_{WV} and TR_O were obtained for the plastic substrate with no additional coating layers. An improvement of the gas-blocking properties by one to three orders of magnitude for water vapor and oxygen is necessary for the plastic substrate to satisfy the requirements for OLED applications (TR_{WV} and TR_O of $<10^{-6}$ g/cm²-day-atm and $<10^{-7}$ cc/cm²-day-atm, respectively).[38,39] To further reduce the TR_{WV} and TR_O through the plastic substrates, several types of low-temperature layers have been deposited on the plastic substrates, and their characteristics have been analyzed. Polypropylene glycol (PPG, ~8.9 µm) was spin-coated and cured at low temperature (Sample PPG). Chromium (~400 Å) and aluminum (~2,000 Å) layers were consecutively deposited by a direct-current, cathode-sputtering method under high vacuum (~10^{-6} mbar) (Sample 400 Å Cr/2,000 Å Al). We also deposited hydrogenated amorphous silicon nitride (a-SiN$_x$:H, ~2,500 Å) (Sample 2,500 Å a-SiN$_x$:H) and amorphous silicon oxide (a-SiO$_x$:H, ~2,500 Å) (Sample 2,500 Å a-SiO$_x$:H) by a low-temperature (120°C), plasma-enhanced chemical vapor deposition (LT-PECVD) method. We also consecutively deposited a-SiN$_x$:H (~1,500 Å) and a-SiO$_x$:H (~1,500 Å) on the plastic substrate by the LT-PECVD method (Sample 1,500 Å a-SiN$_x$:H/1,500 Å a-SiO$_x$:H). The measured TR_{WV} and TR_O for the plastic substrates with several additional coatings are summarized in Table III. For sample PPG, the PPG layer does not help to block the gas transmission through the substrate even though a very thick layer was deposited. The bilayer of chromium and aluminum (Sample 400 Å Cr/2,000 Å Al), the a-SiN$_x$:H layer (Sample 2,500 Å a-SiN$_x$:H), and the combination of a-SiN$_x$:H and a-SiO$_x$:H layers (Sample 1,500 Å a-SiN$_x$:H/1,500 Å a-SiO$_x$:H) showed a very good water-vapor blocking property. For these samples, a decrease of TR_{WV} by more than one order of magnitude has been achieved in comparison with the initial substrate measured. The TR_{WV} values are lower than the detection limit of the measurement setup, which is

1.55×10^{-5} g/cm^2-day-atm. Therefore, to accurately analyze the water-vapor transmission properties of the plastic substrates, a new method, such as a calcium test,[39] should be used. The TR$_O$ is also reduced by one order of magnitude for samples 400 Å Cr/2,000 Å Al, 2,500 Å a-SiN$_x$:H, and 2,500 Å a-SiO$_x$:H. Especially, for sample 1,500 Å a-SiN$_x$:H/ 1,500 Å a-SiO$_x$:H, a very good TR$_O$ (2.53×10^{-7} cc/ cm^2-day-atm) has been achieved in comparison with the initial substrate. From our result, we can conclude that a-SiN$_x$:H and a-SiO$_x$:H layers consecutively deposited on one side of the substrate will reduce the water vapor and oxygen TRs to the acceptable levels for OLED applications.

CONCLUSIONS

The properties of the flexible plastic substrate analyzed in this paper, which are important for OLEDs, are summarized in Table IV. A sheet resistance of about 12–13 Ω/□, an optical transmission of greater than 80% over the visible range, and a surface roughness of 1.4–2.2-nm RMS over $50 \times 50 \ \mu m^2$ have been obtained for the TCE coated on plastic substrates. We also investigated the patterning of the electrode by using laser-based, dry-etching, and wet-chemical etching methods. The surface property and gas-blocking properties of the plastic substrate were analyzed using the contact angle and ASTM methodology, respectively. By additionally depositing a combination of hydrogenated, amorphous silicon-nitride and silicon-oxide layers, the water vapor and oxygen TRs were reduced to less than 10^{-5} g/cm^2-day-atm and about 10^{-7} cc/cm^2-day-atm, respectively. The polymer adhesion to the TCE was enhanced by exposing the TCE surface to UV-ozone treatment. Based on our experimental results, we can conclude that these flexible plastic substrates are acceptable for OLED applications.

ACKNOWLEDGEMENTS

REFERENCES

1. G.E. Jabbour, S.E. Shaheen, M.M. Morrell, B. Kippelen, N.R. Armstrong, and N. Peyghambarian, *Opt. Photonics News* 10, 24 (1999).
2. J.W. Allen, *J. Lumin.* 60/61, 912 (1994).
3. N.D. Young, R.M. Bunn, R.W. Wilks, D.J. McCulloch, S.C. Deane, M.J. Edwards, G. Harkin, and A.D. Pearson, *J. SID* 5/3, 275 (1997).
4. M.J. Lee and C.P. Judge, *Solid State Electron.* 44, 1431 (2000).
5. Y. He and J. Kanicki, *Appl. Phys. Lett.* 76, 661 (1998).
6. Y. Hong, Z. He, S. Lee, and J. Kanicki, *Proc. Int. Soc. Opt. Eng.* 4464, 329 (2002).
7. J. Zhao, S. Xie, S. Han, Z. Yang, L. Ye, and T. Yang, *Phys. Status Solidi A* 184, 233 (2001).
8. M.S. Weaver et al., *Proc. 44th Annual Tech. Conf.–Soc. Vacuum Coaters* (Albuquerque, NM: The Society, 2001), p. 155.
9. J.K. Mahon, J.J. Brown, T.X. Zhou, P.E. Burrows, and S.R. Forrest, *Proc. 42nd Annual Tech. Conf.–Soc. Vacuum Coaters* (Albuquerque, NM: The Society, 1999)), pp. 456–459.
10. P.E. Burrows et al., *Proc. Int. Soc. Opt. Eng.* 4105, 75 (2000).
11. A. Berntsen, Y. Croonen, C. Liedenbaum, H. Schoo, R.-J., Visser, J. Vleggaar, and P. van de Weijer, *Opt. Mater.* 9, 125 (1998).
12. G. Gu, P.E. Burrows, S. Venkatesh, S.R. Forrest, and M.E. Thompson, *Opt. Lett.* 22, 172 (1997).
13. J. Zhao, S. Xie, S. Han, Z. Yang, L. Ye, and T. Yang, *Phys. Status Solidi A* 184, 233 (2001).
14. G. Gustafsson, Y. Cao, G.M. Treacy, F. Kavetter, N. Colaneri, and A.J. Heeger, *Nature* 357, 477 (1992).
15. S.H. Kwon, S.Y. Paik, and J.S. Yoo, *Synth. Met.* 130, 55 (2002).
16. LOFO High Tech Film GmbH, TRANSPHAN OG, http://www.lofo.com/english/products/cast-films/transphan/index.html
17. H.C. Choi, Y.Z. Chu, L.S. Heath, and W.K. Smyth, U.S. patent 6,379,509 (30 April 2002).
18. P.Y.Z. Chu, H.C. Choi, L.S. Heath, C.S. Ko, J. Mack, P. Nagarka, J. Richard, W. Smyth, and J. Wang, *Soc. Info. Display Int. Symp., Dig. Tech. Papers* 29, 1099 (1998).
19. N.S. Lennhoff and J. Ram, *U.S. Patent Published Applications*, publication number 20020182386.
20. Y. Aoshima, M. Miyazaki, K. Sato, Y. Kao, S. Takaki, and K. Adachi, *Jpn. J. Appl. Phys.* 40, 4166 (2001).
21. W. Song, S.K. So, and L. Cao, *Appl. Phys. A* 72, 361 (2001).
22. M.G. Mason, L.S. Hung, C.W. Tang, S.T. Lee, K.W. Wong, and M. Wang, *J. Appl. Phys.* 86, 1688 (1999).
23. C.C. Wu, C.I. Wu, J.C. Sturm, and A. Kahn, *Appl. Phys. Lett.* 70, 1348 (1997).
24. T. Osada, T. Kugler, P. Broms, and W.R. Salaneck, *Synth. Met.* 96, 77 (1998).
25. J.S. Kim, M. Granstrom, R.H. Friend, N. Johansson, W.R. Salaneck, R. Kaik, W.J. Feast, and F. Cacialli, *J. Appl. Phys.* 84, 6859 (1998).
26. D.K. Owens and R.C Wendt, *J. Appl. Polymer Sci.* 13, 1741 (1969).
27. D.H. Kaelble, *J. Adhes.* 2, 66 (1970).
28. D.H. Kaelble, *Physical Chemistry of Adhesion* (New York: Wiley, 1971).
29. Z. Hruska and X. Lepot, *J. Fluorine Chem.* 105, 87 (2000).
30. W.R. Runyan, *Semiconductor Measurements and Instrumentation* (New York: McGraw-Hill, 1975).
31. M.A. Logan, *J. Bell System Technol.* 46, 2277 (1967).
32. J.-H. Lan and J. Kanicki, *J. Electron. Mater.* 25, 1806 (1996).
33. W. Cunningham et al., *J. Phys. D Appl. Phys.* 34, 2804 (2001).
34. H. Hosono, M. Kurita, and H. Kawazoe, *Jpn. J. Appl. Phys.* 37, L1119 (1998).
35. H.-Y. Tsai, H. Yang, C.-T. Pan, and M.-C. Chou, *Proc. Int. Soc. Opt. Eng.* 4230, 156 (2000).
36. ASTM, *Standard Test Method for Oxygen Gas Transmission Rate through Plastic Film and Sheeting Using a Coulometric Sensor,* D3985-95 (West Conshohocken, PA: ASTM, 1995).
37. ASTM, *Standard Test Method for Water Vapor Transmission Rate Through Plastic Film and Sheeting Using a Modulated Infrared Sensor,* F1249-90 (West Conshohocken, PA: ASTM, 1995).
38. P.E. Burrows, G.L. Graff, M.E. Gross, P.M. Martin, M.K. Shi, M. Hall, E. Mast, C. Bonham, W. Bennett, and M.B. Sullivan, *Displays* 22, 65 (2001).
39. G. Nisato, P.C.P. Bouten, P.J. Slikkerveer, W.D. Bennett, G.L. Graff, N. Rutherford, and L. Wiese, *Proc. Asia Display/ IDW '01* (San Jose, CA: Society for Information Display, 2001), pp. 1435–1438.